

## **NOTICE WARNING CONCERNING COPYRIGHT RESTRICTIONS**

The copyright law of the United States [Title 17, United States Code] governs the making of photocopies or other reproductions of copyrighted material. Under certain conditions specified in the law, libraries and archives are authorized to furnish a photocopy or other reproduction. One of these specified conditions is that the reproduction is not to be used for any purpose other than private study, scholarship, or research. If a user makes a request for, or later uses, a photocopy or reproduction for purposes in excess of "fair use," that use may be liable for copyright infringement. This institution reserves the right to refuse to accept a copying order if, in its judgement, fulfillment of the order would involve violation of copyright law. No further reproduction and distribution of this copy is permitted by transmission or any other means.

# Rapid #: -18737456

CROSS REF ID: **1020125**

LENDER: **GZM :: Memorial Library**

BORROWER: **WVU :: Downtown Campus Library**

TYPE: Article CC:CCG

JOURNAL TITLE: Journal of applied polymer science

USER JOURNAL TITLE: Journal of applied polymer science.

ARTICLE TITLE: Study on ink flow of silicone rubber for direct ink writing

ARTICLE AUTHOR: Shao, Y., Han, R., Quan, X., & Niu, K.

VOLUME: 138

ISSUE: 33

MONTH: 09

YEAR: 2021

PAGES: 50819

ISSN: 1097-4628

OCLC #: 38145842

Processed by RapidX: 3/3/2022 7:22:00 AM


---

This material may be protected by copyright law (Title 17 U.S. Code)

---

## ARTICLE

## Study on ink flow of silicone rubber for direct ink writing

Yuanrui Shao | Ruijie Han | Xudong Quan | Kangmin Niu 

School of Materials Science and Engineering, University of Science and Technology Beijing, Beijing, China

**Correspondence**

Kangmin Niu, School of Materials Science and Engineering, University of Science and Technology Beijing, Beijing 100083, China.

Email: niukm@ustb.edu.cn

**Funding information**

Fundamental Research Funds for Central Universities, Grant/Award Number: FRF-TP-18-002A1

**Abstract**

Direct ink writing of soft materials is a very promising technology in 3D printing, and the rheological properties of inks are crucial for successful printing. In this paper, the effect of the rheological properties on the printing process of silicone rubber inks is studied to lay a foundation for the configurations of 3D printing process parameters. Also, the shape retention of the printing filaments is studied to provide a basis for the viscosity deployment of the inks. In addition, by studying the die swell ratio of nano-silica-reinforced silicone rubber inks at normal printing speed, it is found that the die-swell ratio is proportional to the ink's relaxation time. Finally, the influence of the configuration of the short-nozzle on the die swell is investigated, and the concave nozzle has a smaller extrusion swelling effect than the convex nozzle and the conical nozzle, providing new ideas for the adjustment of the filament diameter.

**KEYWORDS**

extrusion, manufacturing, rheology, swelling, viscosity and viscoelasticity

## 1 | INTRODUCTION

Compression molding is widely used in the processing of traditional rubber products. Despite of the advantage of good forming quality, it also has many disadvantages, such as, complex forming process, low forming efficiency, high mold manufacturing cost, and difficult manufacturing of complex hollow structural parts.<sup>1,2</sup> Extrusion molding is also used to fabricate rubber products, which can be continuously molded to improve molding efficiency. However, since it can only process products with a constant cross-section, the application of extrusion molding in rubber processing is limited. In spite of high molding efficiency, injection molding also has some disadvantages similar to compression molding, such as, high mold cost and difficulty in demolding products with complex structures, and so on.<sup>3–7</sup> Apparently, it is more flexible and efficient to process rubber products by 3D printing.

As a flexible material, silicone rubber has excellent mechanical properties and good biocompatibility. It is widely used in the fields of aerospace, medical supplies, and flexible electronics.<sup>8–11</sup> The traditional compression

molding method can hardly meet the demands for processing requirements due to the complex product structure and the flexible product requirements in these fields. The 3D printing molding method is flexible, overcomes the shortcomings of the above molding methods, and has a large application potential in the field of silicone rubber processing molding. Compared with 3D printing of rigid materials, printing of flexible materials is more difficult. However, many scholars have achieved fruitful results through research of 3D printing of flexible materials. Truby<sup>12</sup> introduced 3D printing methods suitable for flexible material processing, and demonstrated the great potential of 3D printing in flexible material processing. He<sup>13</sup> summarized the 3D printing methods of flexible polymer materials, analyzed the advantages and limitations of each method in detail, and exhibited the advantages of direct ink writing (DIW) in multi-material printing. Huang<sup>14</sup> prepared conductive silicone rubber filled with carbon fiber and fabricated a sandwich-type flexible strain sensor using the method of DIW. Zhou<sup>15</sup> used nano-silica as rheological modifier and printed silicone elastomers with the elongation of 2000% by DIW.

Kokkinis<sup>16</sup> used a multi-material printing device and a magnetic auxiliary system for 3D printing of composite materials to produce functional materials with complex microstructures. Lei<sup>17</sup> proposed a new strategy for 3D printing of various thermosetting plastics by using the sodium chloride particles as a printing thickener and curing enhancer. Gardan<sup>18</sup> and Yeh Chin-Ching<sup>19</sup> predicted the development trend and market prospects of 3D printing, respectively. Bui<sup>20</sup> prepared a kind of silicone rubber that can be cured quickly under water, which is very suitable for 3D printing.

In conclusion, the in-depth study of flexible material 3D printing methods, applications, and multi-material printing has demonstrated that DIW is an effective tool for 3D printing of silicone rubber. DIW printing materials are not required to be UV-curable or thermoplastic. The device used for DIW printing is very simple, and can directly write viscoelastic material ink under environmental conditions. A typical DIW device for silicone rubber is shown in Figure 1(a). The key to the success of DIW is the design of the ink with good rheological properties, which mainly depends on the rheological control of ink extrusion and stacking. However, it also faces many dilemmas in 3D printing for silicone rubber. The first difficulty is viscosity control. The silicone rubber inks require low viscosity before printing in order to facilitate material transfer and processing, and high viscosity after extrusion to maintain its shape. The second difficulty is to achieve a high degree of forming accuracy which is determined by the ability to extrude a fine, consistent, and uniform filament of silicone rubber inks. However, silicone rubber inks are non-Newtonian fluids with extrusion swelling and shear thinning effects, so it is difficult to precisely control the silicone rubber filaments.

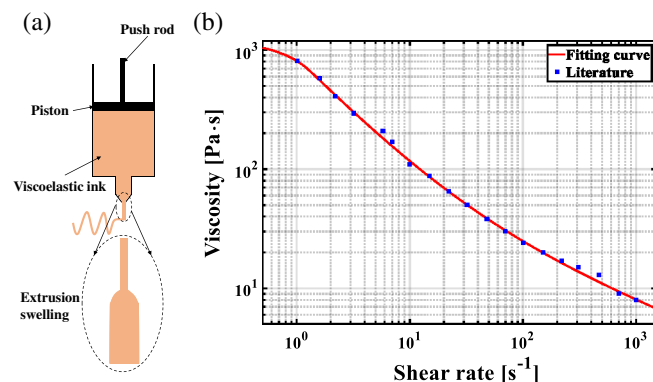


**FIGURE 1** (a) Typical direct ink writing device for silicone rubber and (b) the rheological properties of silicone rubber ink based on the Herschel-Bulkley model [Color figure can be viewed at [wileyonlinelibrary.com](http://wileyonlinelibrary.com)]

DIW is an effective method for flexible material printing, and the rheological properties and the extrusion swelling of the ink seriously affect the molding accuracy of DIW. However, few studies have studied this issue in detail. It is extremely difficult to directly measure the ink flow in the nozzle, but the flow field data in the nozzle can be obtained with the aid of simulation software and accurate rheological data of the ink. Polyflow is a classic commercial software, which has achieved many successful cases in the fields similar to the ink flow in 3D printing such as polymer extrusion processing.<sup>21–24</sup> In this paper, the flows of silicone rubber inks in 3D printing are analyzed by Polyflow software based on the rheological model of inks. What's more, the effects of extrusion swelling under different nozzle configurations is studied, which provides a reference for the selection of parameters and nozzle design for 3D printing. Last but not least, the shape retention of the printing filaments is studied to lay a foundation for the control of ink viscosity.

## 2 | THEORETICAL MODEL

### 2.1 | Fluid governing equations

The flow of ink in the nozzle during 3D DIW printing complies with the following equations.<sup>25,26</sup> The momentum conservation equation is shown in Equation 1.

$$\rho \frac{D}{Dt} \mathbf{V} = \rho \mathbf{f} + \nabla \cdot \mathbf{P} \quad (1)$$

where  $\frac{D}{Dt} = \frac{\partial}{\partial t} + \mathbf{u} \frac{\partial}{\partial x} + \mathbf{v} \frac{\partial}{\partial y} + \mathbf{w} \frac{\partial}{\partial z}$ ,  $\mathbf{V}$  is the velocity vector,  $\rho \mathbf{f}$  is the volume force,  $\mathbf{P}$  is the stress tensor.

The continuity equation (mass conservation equation) of the transient three-dimensional compressible fluid is shown in Equation 2.

$$\frac{\partial \rho}{\partial t} + \nabla \cdot (\rho \mathbf{V}) = 0 \quad (2)$$

If the compression of the ink is very small, it can be generally calculated as an incompressible fluid, and the density  $\rho$  is constant. Then the continuity equation can be simplified to Equation 3.

$$\nabla \cdot \mathbf{V} = 0 \quad (3)$$

The energy conservation equation of fluid is shown in Equation 4.

$$\rho \frac{D}{Dt} \left( e + \frac{v^2}{2} \right) = \rho q + \nabla \cdot (k \nabla T) + \rho \mathbf{f} \cdot \mathbf{V} + \nabla \cdot (\mathbf{P} \cdot \mathbf{V}) \quad (4)$$

The energy conservation equation can be ignored in the case of neglecting heat generated by viscous dissipation of fluid.

The Equation 1, Equation 2, Equation 3, Equation 4 belongs to the classical fluid mechanics formulas based on continuous medium and are valid for both Newtonian and non-Newtonian fluids. The ink's flow during 3D printing is analyzed based on the above theoretical model.

## 2.2 | The ink and flow region model

The ink of DIW is usually formulated as a non-Newtonian fluid with shear thinning properties for the convenience of processing. The inks that cannot be cured quickly by means of light curing should have a certain yield strength. The commonly used shear rate-dependent rheological models include Power Law, Bird-Carreau Law, Cross Law, Bingham Law, Herschel-Bulkley Law, Log-Log Law, Carreau-Yasuda Law, and other models.<sup>27,28</sup>

Power law is the simplest and easiest model to use among the above rheological models, but it cannot well demonstrate the rheological behavior at low shear rates. Bird-Carreau Law and Cross Law can describe the rheological behavior at low shear rates, while Bird-Carreau Law can smooth the transition from Power Law at high shear rates. The properties of Carreau-Yasuda Law are similar to Bird-Carreau Law, and the transition from Carreau-Yasuda to Power law can be adjusted. The Log-Log Law model is a pure empirical fitting model which can obtain a better fitting model with experimental data for some fluids with complex rheological behavior. The Bingham Law model can explain the shear yield strength of materials, but it cannot describe the shear thinning behavior well. The Herschel-Bulkley Law model can not only express the shear yield behavior of materials, but also describe the shear thinning behavior of materials.<sup>29–31</sup>

The RTV (room temperature vulcanized) silicone rubber has the characteristic of shear thinning. However, it has a certain shear yield strength after adding nano-silica as reinforcing agent and generally shows similar rheological behavior<sup>32</sup> with concrete, mud, dough, toothpaste, and so on. Therefore, it is more appropriate to use the Herschel-Bulkley Law model to describe the rheological model of the materials studied.

The Herschel-Bulkley<sup>33</sup> model is usually written as Equation 5.

$$\tau = \tau_0 + k\dot{\gamma}^n \quad (5)$$

where  $\tau$  is the shear stress,  $\tau_0$  is the yield stress,  $k$  is the consistency coefficient,  $\dot{\gamma}$  is the shear rate, and  $n$  is the

flow index. If  $\tau < \tau_0$ , Herschel-Bulkley fluid shows solid-like properties, otherwise it exhibits fluid properties. This characteristic describes the Bingham behavior of Herschel-Bulkley fluid. The Herschel-Bulkley fluid is shear thinning fluid when  $n < 1$ , and shear thickening fluid when  $n > 1$ . When  $n = 1$  and  $\tau_0 = 0$ , the Herschel-Bulkley model degenerates to a Newtonian fluid.

The viscosity of Herschel-Bulkley fluid<sup>34</sup> is given in Equation 6.

$$\mu = \begin{cases} \frac{\tau_0 \left(2 - \frac{\dot{\gamma}}{\dot{\gamma}_0}\right)}{\dot{\gamma}_0} + k \left[ (2-n) + (n-1) \frac{\dot{\gamma}}{\dot{\gamma}_0} \right], & \dot{\gamma} \leq \dot{\gamma}_0 \\ k \left( \frac{\dot{\gamma}}{\dot{\gamma}_0} \right)^{n-1} + \frac{\tau_0}{\dot{\gamma}}, & \dot{\gamma} \geq \dot{\gamma}_0 \end{cases} \quad (6)$$

where  $\mu$  is the viscosity, and  $\dot{\gamma}_0$  is the critical shear rate.

The shear rate and viscosity data of silicone rubber SE1700PDMS are obtained from the literature.<sup>35,36</sup> The fitting result of the viscosity and shear rate of the ink based on the Herschel-Bulkley model is shown in Figure 1(b), and the yield stress  $\tau_0 = 764.01$  Pa, consistency coefficient  $k = 86.977$  Pa · s, flow index  $n = 0.6259$ , critical shear rate  $\dot{\gamma}_0 = 1.316$  s<sup>-1</sup>.

In order to explore the influences of the rheological property of the ink on the printer parameters during the printing process, a nozzle model as shown in Figure 2 is constructed, and its axonometric drawing and dimensions are also shown in Figure 2.

Since the nozzle of 3D printing is a three-dimensional axisymmetric structure, a half-plane model is constructed through the commercial CFD software ANSYS Polyflow according to Figure 2 to calculate the flow field inside the nozzle in order to reduce the amount of calculation. The quadrilateral structured grids are used to divide the fluid domain. The size of the control unit is 0.1 mm, the total number of units is 4060, and the total number of nodes is 4286. The specific grid division is shown in Figure 3.

The boundary conditions of the finite element model are shown in Figure 3(c). The boundary condition A is set as axisymmetric condition, B is set as inlet condition of fully develop fluid, and the value of inlet flow is set to 7.854 mm<sup>3</sup>. according to the printing speed of 10 mm · s<sup>-1</sup>. C is set as the outlet condition, and the normal force and axial force are both zero. D is set as the fixed boundary condition, and the normal velocity and axial velocity are both zero according to the viscosity condition without slip. E is set as the free surface boundary condition, which will automatically adapt to re-meshing during the calculation process. The Picard iteration method is used to solve the flow equation.

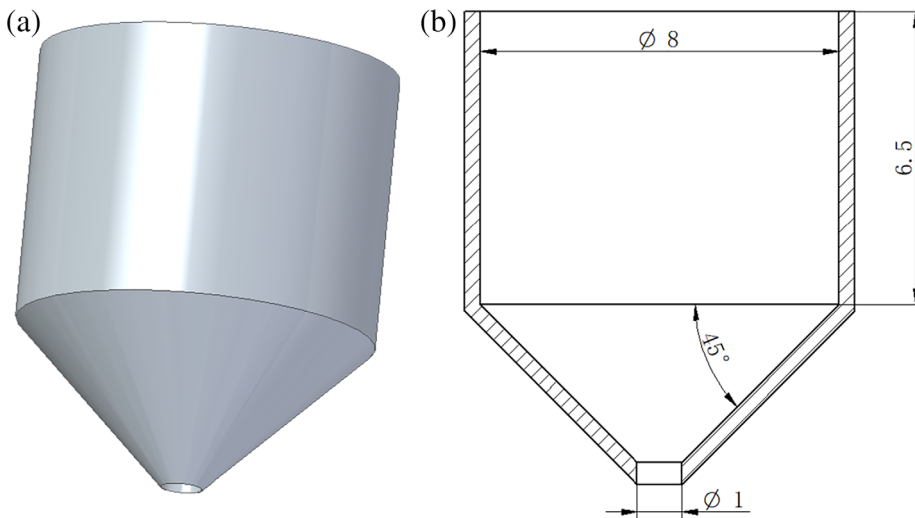


**FIGURE 2** The nozzle of 3D printing for flexible material; (a) axonometric drawing of nozzle; (b) dimensions of nozzle [Color figure can be viewed at wileyonlinelibrary.com]

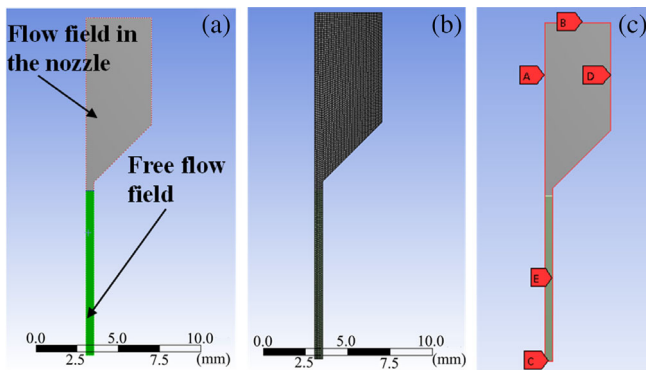


**FIGURE 3** Finite element model of flow field; (a) fluid domain; (b) meshing; (c) boundary conditions [Color figure can be viewed at wileyonlinelibrary.com]

### 2.3 | The cross-section model for filament of 3D printing

The ink can be considered as a Bingham fluid represented by the Herschel-Bulkley model. If the pressure at the bottom of the filament  $P \leq \tau_0$ , that is, the driving force of fluid flow is less than the shear yield stress, there will be no flow at the bottom of the filament. However, the contact stress is greater than  $\tau_0$  when the filament extruded by the print nozzle is just laid on the bottom plate because of the small contact area. This will cause flow at the bottom of the filament. The contact area gradually increases with the flow of the filament at the bottom. Finally, the contact stress is equal to  $\tau_0$ , and the fluid reaches an equilibrium state. As shown in Figure 4, the cross-section of the filament becomes a peculiar shape with a circular upper part and a trapezoidal lower part.

The effect of surface tension can be ignored, when  $\tau_0$  is relatively large. The filament height  $h$  is divided into

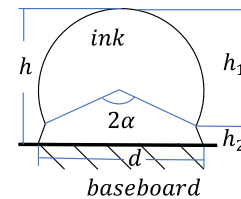


**FIGURE 4** The cross-sectional shape of the Bingham ink filaments [Color figure can be viewed at wileyonlinelibrary.com]

the upper height  $h_1$  and the lower platform height  $h_2$ . The flow driving force in the upper part is less than the shear yield stress, so the dimension of it is consistent with the initial size of the filament according to the properties of the Herschel-Bulkley fluid. The height  $h_1$  can be calculated by geometrical relations. The ink which can be described as the Herschel-Bulkley fluid in the lower part can flow because the contact stress is greater than the shear yield stress. The lower part of the circular section of the filament becomes a trapezoid, and the pressure on the upper and lower surfaces of the trapezoidal platform is equal to the shear yield stress.

The pressure of the upper and lower surface of the trapezoidal platform when the fluid reaches an equilibrium state can be expressed as Equation 7.

$$P = \frac{\rho g V_u}{S_u} = \frac{\rho g R^2 (\pi - \alpha + \sin \alpha \cdot \cos \alpha)}{2R \cdot \sin \alpha} = \frac{\rho g V}{S_b} = \frac{\rho g \pi R^2}{d} = \tau_0 \quad (7)$$

where  $R$  is initial radius of filament,  $S_u$  is upper surface area of trapezoidal platform at the bottom of filament per unit length,  $S_b$  is lower surface area, and  $d$  is the width of the lower surface.

So, the  $d$  can be expressed as Equation 8.



$$d = \frac{\rho g \pi R^2}{\tau_0} \quad (8)$$

$$\frac{\pi - \alpha + \sin \alpha \cdot \cos \alpha}{2 \sin \alpha} = \frac{\tau_0}{\rho g R} \quad (9)$$

Then the height of the filament can be expressed as Equation 10 and Equation 11.

$$h_2 = \frac{2R^2(\alpha - \sin \alpha \cdot \cos \alpha)}{d + 2R \cdot \sin \alpha} \quad (10)$$

$$h = h_1 + h_2 = R + R \cdot \cos \alpha + \frac{\tau_0 R(\alpha - \sin \alpha \cdot \cos \alpha)}{\rho g \pi R + 2\tau_0 \cdot \sin \alpha} \quad (11)$$

The height of the Herschel-Bulkley type ink filament can be obtained by combining Equation 9 and Equation 11.

### 3 | RESULTS AND DISCUSSION

#### 3.1 | Computational fluid dynamics analysis of ink flow

The ink's flow in the nozzle is shown in Figure 5. Overall, the pressure, flow rate, and shear rate in the nozzle are relatively constant in the upper part of the nozzle, but there is a large gradient at the exit of the nozzle.

It can be seen from Figure 5(a) that the pressure of ink drops to zero instantaneously after it flows out of the nozzle and a large pressure difference is formed between inside and outside the nozzle outlet. The negative

pressure is formed at the nozzle exit due to the discontinuity of flow boundary conditions at the nozzle exit according to the magnified figure. The secondary flow of the ink caused by the negative pressure will bring bubbles to it, which will affect the quality of 3D printing.

It can be seen from Figure 5(b) that there are great changes of the velocity field of the ink near the nozzle outlet. As the distance from the outlet decreases, the velocity of the ink gradually increases. At the moment of ejecting, the maximum velocity will be reached. After leaving the nozzle for 10 mm, the ink's velocity will be reduced to level off. As can be seen in the magnified view of the nozzle in Figure 5(b), the velocity of the ink near the axis decreases significantly when it just comes out of the nozzle, while the velocity of the ink outside increases remarkably. The direction of the velocity vector of ink at the outlet is backward to the axis of symmetry and points to the normal direction, which causes the fluid particles to move towards the free surface, forming an extrusion swelling effect. As shown in Figure 5(c), the shear rate of the ink in most areas of the nozzle is small, and it gradually increases near the outlet. When the shear rate of the ink at the outlet exceeds the critical shear rate ( $1.316 \text{ s}^{-1}$ ), it exhibits the characteristic of shear thinning which improves the processability of the ink. As shown in Figure 5(d), the flow rate of ink near the center axis in the nozzle is larger than the one closer to the outside and the contour of the flow function in the figure is the streamline of ink. The streamline of ink inside the nozzle, which is approximately parallel to the inside wall of the nozzle, turns at the point of contraction of the inside wall of the nozzle, which may form a secondary backflow.

From the analysis of the entire flow field, the flow rate of ink in the area around the center axis accounts for

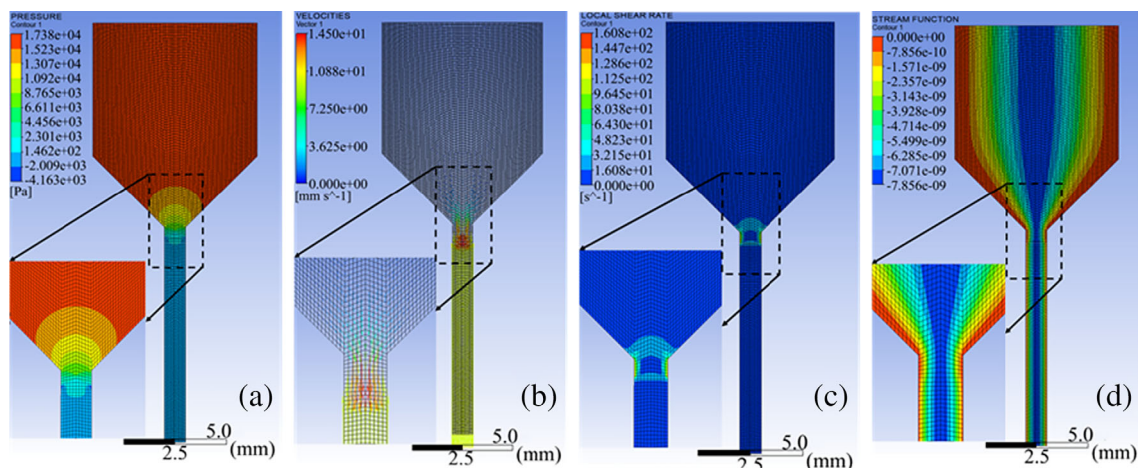


FIGURE 5 Analysis of ink flow inside the nozzle; (a) pressure distribution; (b) flow velocity distribution; (c) shear rate distribution; (d) flow function in the nozzle [Color figure can be viewed at [wileyonlinelibrary.com](http://wileyonlinelibrary.com)]

most of the flow, while the flow rate in the area about 5 mm closer to the nozzle wall is almost zero. That is to say, there is a part of the fluid static area in the nozzle, which is very unfavorable for printing of flexible materials such as silicone rubber that slowly vulcanize at room temperature. As the printing time increases, the mixed silicone rubber will slowly vulcanize in non-flowing area of the nozzle, increase the propulsion resistance, and eventually block the printing nozzle to interrupt printing. Therefore, the nozzle configuration needs to be optimized to minimize the non-flowing area.

In order to improve the shape retention of the silicone rubber ink, it is generally necessary to have it modified, such as adding nano-silica fillers to increase its shear yield stress  $\tau_0$ . The relationship between propulsion pressure and shear yield strength of ink was analyzed in Figure 6(a).

As shown in Figure 5(c), the shear rate of the ink in the nozzle except for the outlet is lower than the critical shear rate. The ink's viscosity at the nozzle outlet reduces due to the shear thinning effect while it remains steady at the rest of the nozzle according to the analysis of Equation 6. Therefore, the rheological properties of the Herschel-Bulkley type ink are close to the Newtonian fluid with constant viscosity at low shear rate. As shown in Figure 6(a), propulsion pressure shows a linear increase with the increase of shear yield strength of the ink.

The relationship between extrusion speed and propulsion pressure is shown in Figure 6(b). It can be seen that the propulsion pressure increases continuously with the increase of extrusion speed. However, the slope of the curve decreases with extrusion speed. This is because at higher extrusion rates, there will be more areas where the shear rate exceeds the critical shear rate  $\dot{\gamma}_0 (1.316 \text{ s}^{-1})$  in the flow field, and shear thinning of ink appears in more flow areas.

### 3.2 | The effect of rheology of ink on extrusion swell

The size of the extruded filaments will be larger than that of the nozzle during the DIW process, and this phenomenon of polymer extrusion swelling is called Barus effect.<sup>29</sup> The nozzle used in DIW generally has a circular outlet, and the ratio of the diameter of the extrudate to the diameter of the extrusion die can be used to indicate the degree of extrusion expansion. This ratio is usually called the extrusion swell ratio,<sup>37</sup> which is represented by  $B$  in Equation 12.

$$B = \frac{D_e}{D} \quad (12)$$

where  $D_e$  is the diameter of the extruded filament, and  $D$  is the diameter of nozzle's outlet. The rheological properties of ink, the extrusion speed, the nozzle outlet diameter, and the shape of the flow channel in the nozzle will all affect the extrusion swell ratio according to a large number of studies.<sup>38</sup>

As mentioned above, the shear yield stress of ink can be increased through adding nano-silica in order to improve the shape retention. However, the ink will show more obvious viscoelastic characteristics with the addition of these nanoparticles.<sup>39,40</sup> This will significantly increase the extrusion swell effect of the ink, which has a great impact on the printing accuracy. Therefore, it is very necessary to study the relationship between the rheological properties of ink and the extrusion swell.

The generalized Newtonian fluid models, such as the Herschel-Bulkley model, can no longer accurately describe the rheological behavior of viscoelastic inks since the addition of nanoparticles improves the elasticity of them.<sup>41</sup> In order to better characterize the extrusion swelling effect, it is necessary to select a suitable

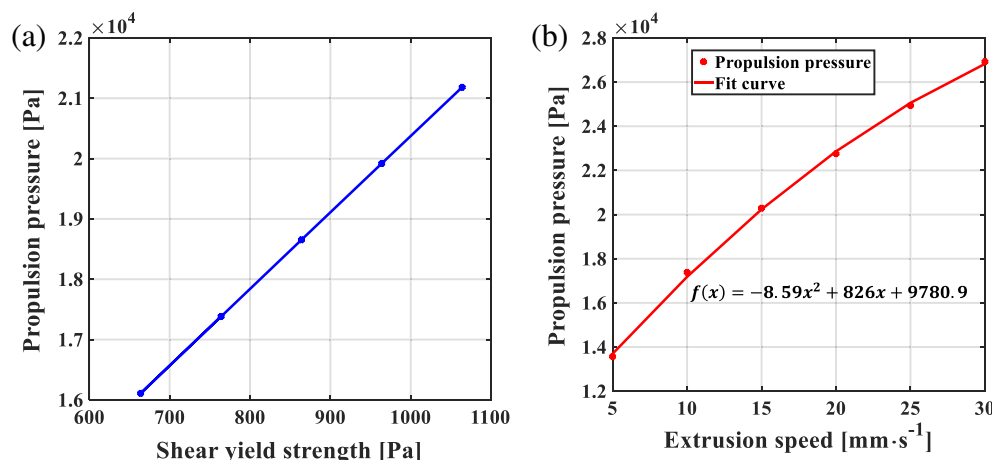


**FIGURE 6** The relationship between printing parameters and ink's rheology; (a) shear yield stress and propulsion pressure; (b) extrusion speed and propulsion pressure [Color figure can be viewed at [wileyonlinelibrary.com](http://wileyonlinelibrary.com)]



viscoelastic model based on experimental data such as viscosity-shear rate curve, storage modulus curve and loss modulus curve.

Among the models characterizing the viscoelasticity of polymer solutions, the FENE-P model derived from

molecular theory is suitable for describing the viscoelastic behavior of dilute solutions and has a physical model similar to the silicone rubber ink. The model can predict the shear thinning and the first normal stress difference of the real viscoelastic fluid.<sup>42,43</sup> Therefore, it can better describe the extrusion swelling effect than the generalized Newtonian fluid models.

The FENE-P model idealizes the polymer solution as dumbbell-shaped polymer macromolecules connected by springs suspended in a Newtonian viscosity solvent and it can be expressed as Equation 13.

$$\tau = \frac{\eta}{\lambda} \left( \frac{A}{1 - \text{tr}(A)L^{-2}} - \frac{I}{1 - 3L^{-2}} \right) \quad (13)$$

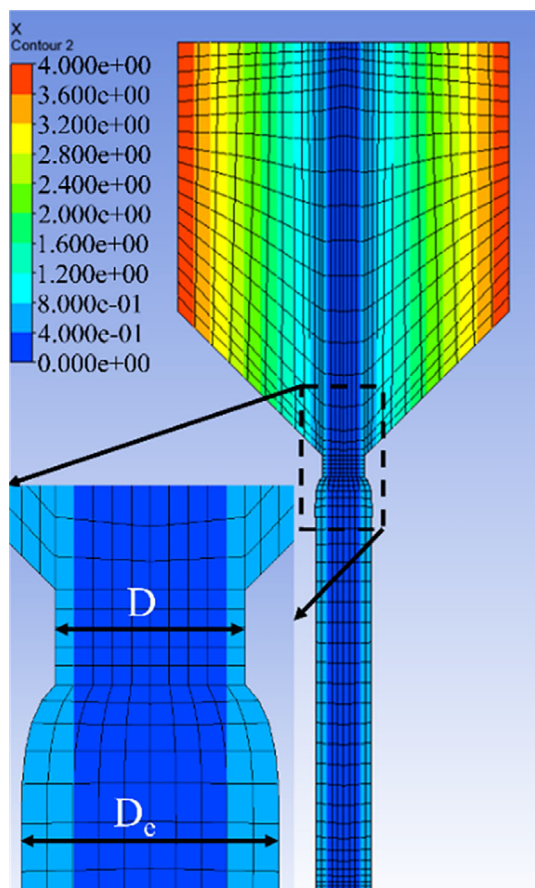


FIGURE 7 Extrusion swell of ink [Color figure can be viewed at wileyonlinelibrary.com]

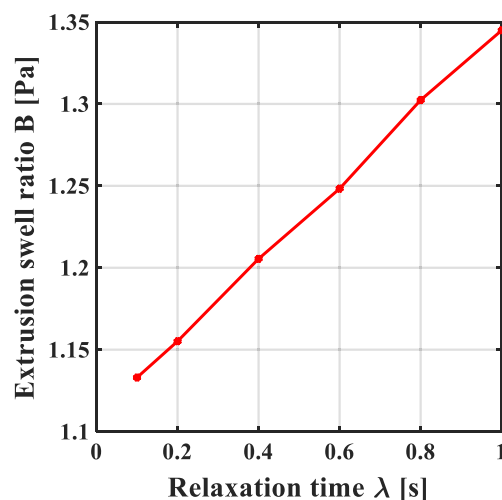


FIGURE 9 The relationship between the extrusion swell ratio and the relaxation time of the ink [Color figure can be viewed at wileyonlinelibrary.com]

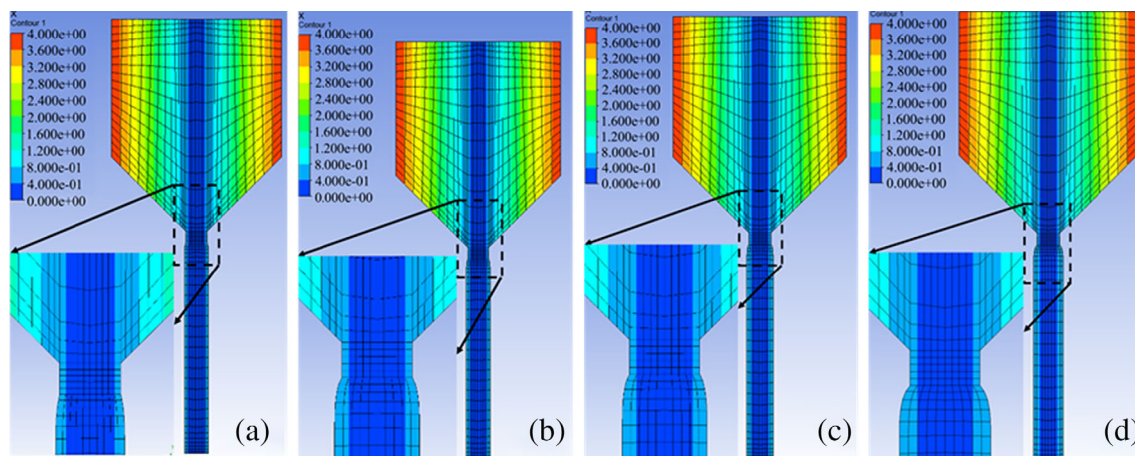
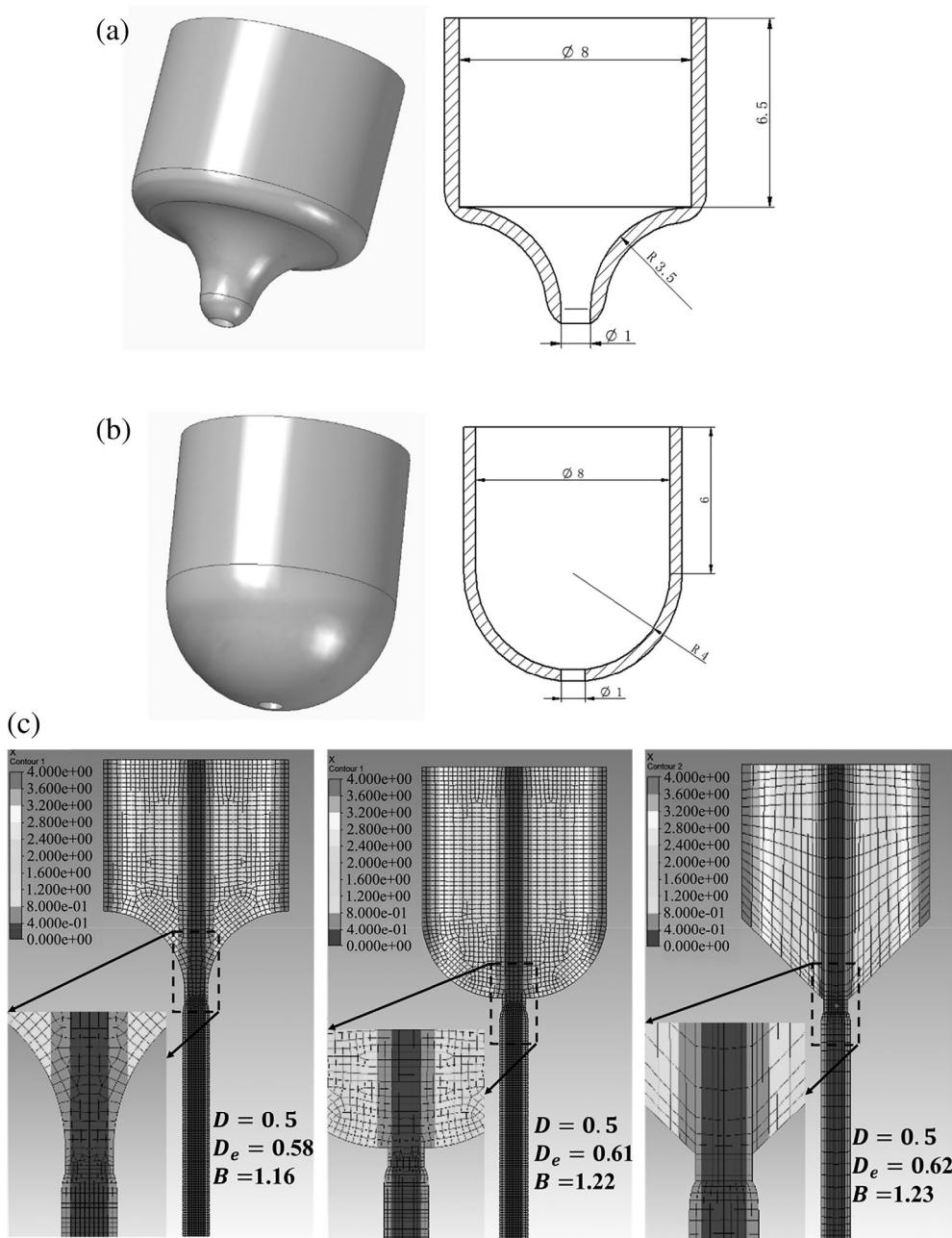


FIGURE 8 Extrusion swell of ink under different relaxation time; (a)  $\lambda = 0.1$ ; (b)  $\lambda = 0.2$ ; (c)  $\lambda = 0.4$ ; (d)  $\lambda = 0.8$  [Color figure can be viewed at wileyonlinelibrary.com]



**FIGURE 10** Extrusion swelling of ink under different nozzle configurations; (a) [Color figure can be viewed at [wileyonlinelibrary.com](http://wileyonlinelibrary.com)]

where  $A$  is calculated as follows.

$$\frac{A}{1 - \text{tr}(A)L^{-2}} + \lambda_A^{\nabla} = \frac{I}{1 - 3L^{-2}} \quad (14)$$

and  $\tau$  is the shear stress,  $\eta$  is the viscosity,  $\lambda$  is the relaxation time,  $I$  is the unit tensor, and  $L$  is the ratio of the maximum length of the spring to the relaxation length.

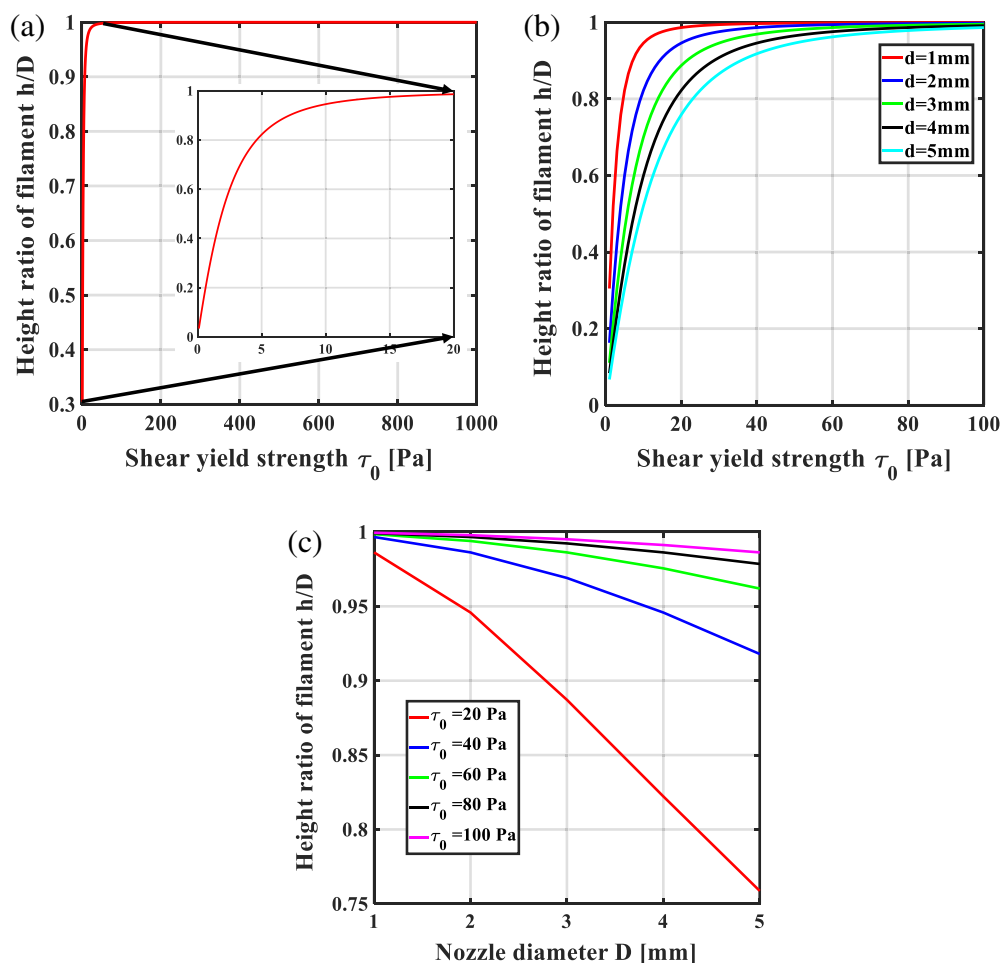
$$L^2 = \frac{R_0^2}{R_e^2} \quad (15)$$

The experimental data of silicone rubber ink containing 8 wt % nano-silica in the literature<sup>15</sup> was used to fit the

FENE-P model through the Polymat software and the fitting result was  $\eta=320$ ,  $\lambda = 1$ ,  $L = 2.889$ . Then, the material parameters obtained by fitting were introduced into the finite element model established in Section 2.2 to get the extrusion swell ratio of the filament and the deformation of filament was shown in Figure 7. It can be obtained from the CFD post-processing software that  $D = 0.5$ ,  $D_e = 0.67246$  mm. Finally, the parameter  $B = 1.345$  was calculated by Equation 12.

The extrusion swelling of the ink with relaxation time changes from 0.1 to 0.8 is shown in Figure 8. It can be seen that the extrusion swelling effect becomes more obvious with the increase of relaxation time. This is because the elasticity of the ink increases as the relaxation time increases, and the fluid model of the ink

**FIGURE 11** Effects of shear yield strength and nozzle diameters on height ratio of filament; (a)  $D = 1$  mm; (b) the height ratio of filament under different nozzle diameters; (c) the height ratio of filament under different shear yield strength of ink [Color figure can be viewed at [wileyonlinelibrary.com](http://wileyonlinelibrary.com)]



gradually changes from a generalized Newtonian fluid to a viscoelastic fluid. The effect of the viscoelasticity of the ink on the extrusion swelling was illustrated quantitatively in Figure 9 and the extrusion swell ratio is directly proportional to the relaxation time of the ink at a certain printing speed.

### 3.3 | The influence of nozzle configuration on extrusion swell

The extrusion swelling of ink will affect the selection of printing parameters and the printing accuracy. In order to analyze the relationship between different configuration nozzles and extrusion swelling, the concave nozzle and convex nozzle model with the same flow channel length as the cone nozzle are established. The specific dimensions of models are shown in Figure 10(a) and Figure 10(b). Then, the CFD analysis of extrusion swelling is carried out using the models with  $\lambda = 0.5$  and the boundary condition setting and meshing method are the same as those mentioned in Section 2.2.

Concave nozzle; (b) Convex nozzle; (c) The extrusion swell ratio.

As shown in Figure 10(c), the extrusion swelling of the ink is affected by nozzle configuration. The extrusion swell ratio of the convex and conical nozzles is similar, while the extrusion expansion effect of the concave nozzle is smaller. The reason for this is that the ink is squeezed by the inner wall of the concave nozzle. The flow line will converge earlier, thus reducing the extrusion swell effect. On the other hand, the extrusion section of the inner wall of the nozzle against the ink is longer, so that the first normal stress difference of the extruded filament is smaller, and the elastic expansion after extrusion is also reduced.

### 3.4 | The influence of rheological properties of ink on the laying height of filament

The laying height of filament  $h = 0.999$  mm can be obtained from Equation 9 and Equation 11 as the density of ink is  $1.05 \text{ g} \cdot \text{ml}^{-1}$ , nozzle diameter is 1 mm, and shear yield strength is  $\tau_0 = 764.01$  Pa. The height ratio on the shape retention of the filament is defined as the ratio of the height of the filament to the nozzle diameter,  $h/D$ ,

and it indicates the formability of ink. The change of height ratio of filament with the shear yield strength is shown in Figure 11(a). It can be seen from the figure that the height ratio of filament increases rapidly as the shear yield strength increasing when  $\tau_0$  is less than 30 Pa, and height ratio of filament can reach above 0.95 when the shear yield strength is greater than 20 Pa according to the magnified figure.

Figure 11(b) and Figure 11(c) show the effects of shear yield strength and nozzle diameters on height ratio of filament, respectively. As can be seen from Figure 11(b), with shear yield strength increasing, height ratio of filament under different nozzle diameters becomes significantly larger, but the growth rate becomes slower. Figure 11(c) shows that the height ratio of filament gradually decreases as the nozzle diameter increasing, but the decline rate becomes faster with the decreasing shear yield strength. The above analysis provides the insights for ink preparation with different nozzles. The appropriate shear yield strength can be selected from Figure 11(b) with the certain nozzle diameter and corresponding shape retention requirements. In the case of meeting the requirements of shape retention, the smaller the shear yield strength is, the more favorable it is for printing.

## 4 | CONCLUSION

The 3D printing for soft materials is still immature, and there are still many problems to be solved. In this study, the ink flow model and cross-section model for filament were constructed to study the issue of the shape retention of printing filaments and the selection of printing parameters. The main conclusions of this study are as follows:

1. The rheological properties of the Herschel-Bulkley type ink are close to the Newtonian fluid with constant viscosity at low shear rate, so the propulsion pressure is approximate proportional to extrusion speed and shear yield strength when the extrusion speed is less than  $30 \text{ mm s}^{-1}$ .

2. The extrusion swell effect of ink becomes more obvious with the increase of relaxation time, and the extrusion swell ratio is directly proportional to the relaxation time of the ink at a certain printing speed.

3. The extrusion swell rate of the convex nozzle and the conical nozzle is similar, but the concave nozzle has a smaller extrusion swell effect, so the selection of the concave nozzle can reduce the influence of the extrusion swell effect on the printing accuracy.

4. The shear yield strength of the ink and the nozzle diameter has a greater impact on the shape retention of the filament. The height ratio of filament increases with

the increase of shear yield strength and decreases with the increase of nozzle diameter. This study provides reference for ink preparation, for example, the shear yield strength needs to be above 20 Pa to achieve good shape retention when the nozzle diameter is 1 mm.

## ACKNOWLEDGMENT

The authors wish to thank the Fundamental Research Funds for the Central Universities (FRF-TP-18-002A1) for supporting this research.

## CONFLICT OF INTEREST

The authors declare no potential conflict of interest.

## ORCID

Kangmin Niu  <https://orcid.org/0000-0001-7554-7754>

## REFERENCES

- [1] Y. Dong, H. Yang, H. Yan, X. Yao, *Compos. Struct.* **2019**, 229, 111463.
- [2] Y. Ke, X. Yao, H. Yang, X. Liu, *Tribol. Int.* **2014**, 72, 35.
- [3] G. Ramorino, M. Girardi, S. Agnelli, A. Franceschini, F. Baldi, F. Viganò, T. Riccò, *Int. J. Mater. Form.* **2010**, 3, 551.
- [4] J. S. Deng, A. I. Isayev, *Rubber Chem. Technol.* **1991**, 64, 296.
- [5] K. Maghsoudi, R. Jafari, G. Momen, M. Farzaneh, *Mater. Today Commun.* **2017**, 13, 126.
- [6] T. Hutterer, G. R. Berger-Weber, R. C. Kerschbaumer, W. Friesenbichler, *Polym. Eng. Sci.* **2020**, 61, 1. <https://doi.org/10.1002/pen.25604>.
- [7] Z. X. Xin, Z. X. Zhang, K. Pal, J. U. Byeon, S. H. Lee, J. K. Kim, *Mater. Des.* **2010**, 31, 589.
- [8] D. B. B. Gans, P. C. Duineveld, U. S. Schubert, *Adv. Mater.* **2004**, 16, 203.
- [9] Q. He, A. Li, Y. Zhang, S. Liu, Y. Guo, L. Kong, *Tribol. Mater. Surf. Interfaces* **2018**, 12, 9.
- [10] H. Yang, X. Yao, L. Yuan, L. Gong, Y. Liu, *Nanoscale* **2019**, 11, 578.
- [11] H. Yang, X. Yao, Z. Zheng, L. Gong, L. Yuan, Y. Yuan, Y. Liu, *Compos. Sci. Technol.* **2018**, 167, 371.
- [12] R. L. Truby, J. A. Lewis, *Nature* **2016**, 540, 371.
- [13] L.-Y. Zhou, J. Fu, Y. He, *Adv. Funct. Mater.* **2020**, 30, 2000187.
- [14] P. Huang, Z. Xia, S. Cui, *Mater. Des.* **2018**, 142, 11.
- [15] L. Zhou, Q. Gao, J. Fu, Q. Chen, J. Zhu, Y. Sun, Y. He, *ACS Appl. Mater. Interfaces* **2019**, 11, 23573.
- [16] D. Kokkinis, M. Schaffner, A. R. Studart, *Nat. Commun.* **2015**, 6, 8643.
- [17] D. Lei, Y. Yang, Z. Liu, S. Chen, B. Song, A. Shen, B. Yang, S. Li, Z. Yuan, Q. Qi, *Mater. Horizons* **2019**, 6, 394.
- [18] J. Gardan, *Int. J. Prod. Res.* **2016**, 54, 3118.
- [19] C. Yeh, *Int. J. Autom. Smart. Technol.* **2014**, 4, 1.
- [20] R. Bui, M. A. Brook, *Adv. Funct. Mater.* **2020**, 30, 2000737.
- [21] M. K. Choudhary, J. A. Kulkarni, *Polym. Eng. Sci.* **2008**, 48, 1177.
- [22] X. H. Gan, Q. Liu, X. J. Ma, N. N. Liu, C. C. Yang, *Adv. Mat. Res.* **2012**, 354-355, 642.
- [23] K. Liu, D. Grecov, *Appl. Math. Model.* **2011**, 35, 1603.
- [24] J. S. Wen, X. L. Zhou, *Appl. Mech. Mater.* **2012**, 220-223, 1719.



- [25] H. A. Barnes, J. F. Hutton, K. Walters, *An Introduction to Rheology*, Elsevier, Amsterdam **1989**.
- [26] V. Girault, P. Raviart, *Finite Element Methods for Navier-Stokes Equations: Theory and Algorithms*, Springer, New York, NY **1986**.
- [27] A. I. Leonov, *J. Nonnewton. Fluid. Mech.* **1992**, 42, 323.
- [28] Simhambhatla, M. V. The rheological modeling of simple flows of unfilled and filled polymers, PhD Thesis, University of Akron, **1994**.
- [29] R. Cherizol, M. Sain, J. Tjong, *Green Sustainable Chem.* **2015**, 05, 6.
- [30] I. Ansys, *ANSYS Polyflow User's Guide*, Ansys Inc, Canonsburg, PA **2012**.
- [31] H. H. Winter, M. Mours, *Adv. Polym. Sci.* **1997**, 134, 165.
- [32] A. C. Wong, A. C. M. Wong, *Polym. Test.* **2018**, 71, 262.
- [33] W. H. Herschel, R. Bulkley, *Kolloid-Zeitschrift.* **1926**, 39, 291.
- [34] K. C. Sahu, P. Valluri, P. D. M. Spelt, O. Matar, *Phys. Fluids* **2007**, 19, 122101.
- [35] X. Zhu, Y. Chen, Y. Liu, Y. Deng, C. Tang, W. Gao, J. Mei, J. Zhao, T. Liu, J. Yang, *Rapid Prototyp. J.* **2018**, 24, 1579.
- [36] X. Zhu, Y. Chen, Y. Liu, C. Tang, T. Liu, J. Mei, W. Gao, J. Yang, *Appl. Phys. A: Mater. Sci. Process.* **2019**, 125, 247.
- [37] J. Brandao, E. Spieth, C. Lekakou, *Polym. Eng. Sci.* **1996**, 36, 49.
- [38] R. I. Tanner, *J. Nonnewton. Fluid. Mech.* **2005**, 129, 85.
- [39] A. B. Metzner, *J. Rheol.* **1985**, 29, 739.
- [40] Q. D. Nguyen, D. V. Boger, *Annu. Rev. Fluid Mech.* **1992**, 24, 47.
- [41] M. Crochet, R. Keunings, *J. Nonnewton. Fluid. Mech.* **1982**, 10, 339.
- [42] R. B. Bird, P. J. Dotson, N. L. Johnson, *J. Nonnewton. Fluid. Mech.* **1980**, 7, 213.
- [43] B. Robertson, R. L. Thompson, T. C. B. McLeish, I. Robinson, *J. Rheol.* **2019**, 63, 319.

**How to cite this article:** Shao Y, Han R, Quan X, Niu K. Study on ink flow of silicone rubber for direct ink writing. *J Appl Polym Sci.* 2021;138: e50819. <https://doi.org/10.1002/app.50819>